Benefits of using the high-resolution linear radon transform (HRLRT) with the multi-channel analysis of surface waves (MASW) method

Julian Ivanov, Richard D. Miller, Daniel Z. Feigenbaum, Kansas Geological Survey; and J. Tyler Schwenk, Primal Innovation*

Summary

We evaluate the benefits of the use of the high-resolution linear radon transform (HRLRT) with the multi-channel analysis of surface waves (MASW) seismic method. Love- and Rayleigh-wave synthetic and real-world seismic data from both active and passive sources were use to compare dispersion-curve imaging and estimations (an essential MASW component) using both conventional and HRLRT approaches. Results show that benefits from using the HRLRT can include better separation between surface-wave modes, the ability to observe dispersion-curve trends in extended frequency ranges, improved lateral resolution from the ability to use shorter receiver spreads, improved vertical resolution (by using more layers, e.g., 20) from multi-mode inversion, wider passive-data frequency-range and higher-resolution dispersion imaging, reduced spatial aliasing noise, etc.. In such a manner the HRLRT can be a valuable tools in the application of the MASW method on various seismic data sets.

Introduction

The MASW method was initially developed to estimate near-surface shear-wave velocity from high-frequency (≥ 2 Hz) Rayleigh-wave data (Song et al., 1989; Park et al., 1998; Miller et al., 1999b; Xia et al., 1999). Shear-wave velocities estimated using MASW have been reliably and consistently correlated with drill data. Using the MASW method, (Xia et al., 2000) noninvasively measured Vs within 15% of Vs measured in wells. Miller et al. (1999b) mapped bedrock with 0.3-m (1-ft) accuracy at depths of about 4.5-9 m (15-30 ft), as confirmed by numerous borings.

The MASW method has been applied to problems such as characterization of pavements (Ryden et al., 2004), the study of Poisson's ratio (Ivanov et al., 2000a), study of levees (Ivanov et al., 2017) , investigation of sea-bottom sediment stiffness (Ivanov et al., 2000b; Kaufmann et al., 2005; Park et al., 2005), mapping of fault zones (Ivanov et al., 2006a), study of Arctic ice sheets (Tsoflias et al., 2008) and subglacial sediments (Tsuji et al., 2012), and detection of dissolution features (Miller et al., 1999a). Applications of the MASW method have been extended to determination of near-surface quality factor Q (Xia et al., 2013) and the acquisition of more realistic compressional-wave refraction models (Ivanov et al., 2006b; Piatti et al., 2013). A review of established approaches of surface wave methods (SWM) can be found in Socco et al. (2010). Most recent developments of the SWM include the expansion with the use of the horizontal component of the Rayleigh wave (Boaga et al., 2013) and the Love-waves (Dal Moro et al., 2015), evaluation of density information on Rayleigh-wave inversion results (Ivanov et al., 2016), evaluation at landfill sites (Suto, 2013), understanding fault geometry (Ikeda et al., 2013).

The MASW method has three distinct steps. Data acquisition is straight forward and results in a single seismic-data record or shot gather. These seismic traces in the shot gather are transformed into a dispersion-curve image, using the phase-shift method (Park et al., 1998) or the HRLRT (Luo et al., 2008). This image is used to pick a dispersion-curve trend(s) of the Rayleigh wave, which is then inverted to produce a 1-D Vs model (Xia et al., 1999). The Vs(z) profile from each shot gather can be displayed below each shot position to give either a 2-D (Miller et al., 1999b) or 3-D (Miller et al., 2003) estimate of the subsurface V(x, y, z)s model.

Developments in the use of the high-resolution linear radon transform (HRLRT) for dispersion-curve imaging (Luo et al., 2008) have been preferred by many researchers (Zeng et al., 2012; Pan et al., 2013; Ivanov et al., 2017) over conventional algorithms.

We show that the HRLRT can contribute to the better separation between surface-wave modes, the ability to identify and follow dispersion-curve trends in wider frequency ranges, improvement of the lateral resolution from the quality to provide dispersion-curve images with sufficiently high-resolution to interpret and follow fundamental and higher surface-wave modes using shorter receiver spreads, and observe passive data dispersion-curve trends when other methods fail. The HRLRT can also help obtain deeper Vs inversion results with better vertical resolution. This is possible when the HRLRT can assist with the accurate interpretation of higher-modes, which can increase the maximum depth of investigation and obtain stable inversion results by using more layers (e.g., 20 vs 10), from multi-mode inversion. HRLRT can facilitate mode interpretation by reducing spectral leakage.

The Method

We used synthetic and real-world Love- and Rayleigh-wave active-source seismic data set as well as seismic data from passive sources. Each raw seismic data record was converted into two dispersion-curve images using SurfSeis software developed by the Kansas Geological Survey. The first image was obtained using the phase-shift method (Park et al., 1998),

which is referred to from here on as "conventional ". The second image was calculated by using the HRLRT. The ability to observe, interpret, and estimate surface-wave modes in the widest possible frequency range was evaluated on both types of images.

Results

2-layer velocity model synthetic seismic data (Xu et al., 2007; Luo et al., 2008) shows sharper dispersion-curve trends, better separation between fundamental and higher modes, and better match at low frequencies between the calculated and imaged fundamental-mode trend when using the HRLRT image in comparison to the conventional-algorithm image Figure 1).

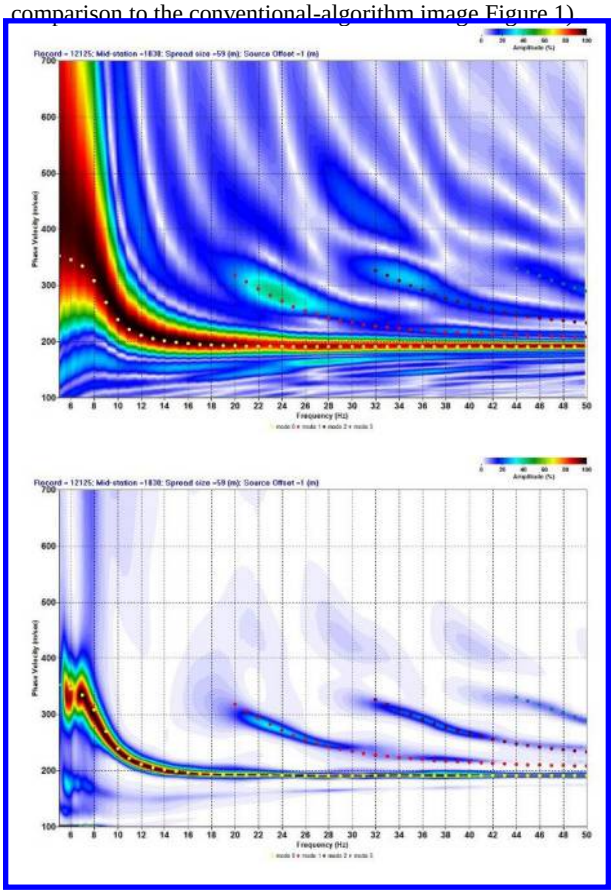

Figure 1. Rayleigh-wave dispersion-curve images of a 2-layer model synthetic seismic data using a) the phase-shift method and b) the HRLRT. Circles indicate calculated fundamental (yellow) and higher mode (other colors) values.

Processing seismic data collected near Garland, Michigan with the conventional dispersion-curve algorithm resulted in obtaining nearly useless images (Figure 2a) with fundamental and higher modes blending into each other (Ivanov et al., 2005). The corresponding HRLRT image provides a clear separation of the fundamental mode from higher modes (Figure 2b).

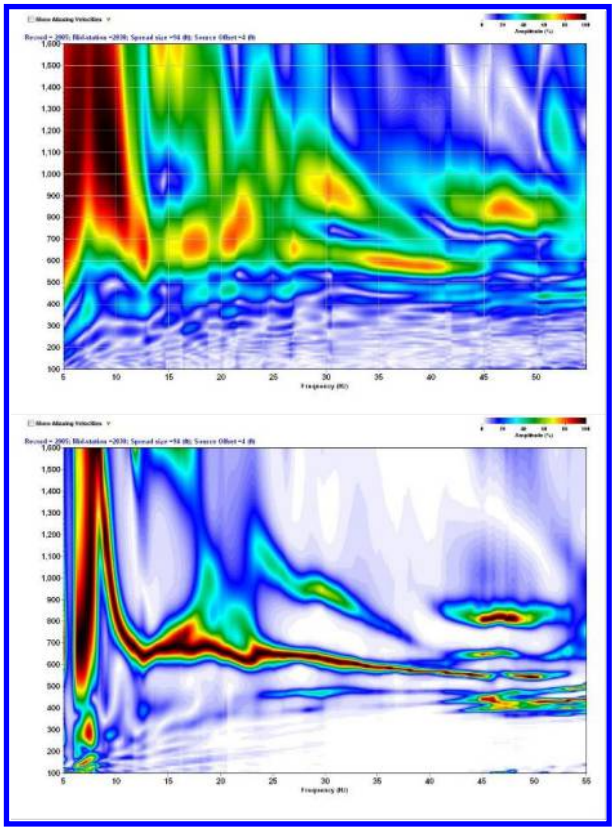

Figure 2. Rayleigh-wave dispersion-curve images of Garland, Michigan seismic data record 2005 using a) the phase-shift method and b) the HRLRT.

Applying the conventional dispersion-curve algorithm on seismic data acquired in Yuma, Arizona (Feigenbaum et al., 2016) resulted in imaging a fundamental mode trend missing the high frequencies >35Hz (Figure 3a), which were needed to estimate the very shallow part of the near-surface section. Using the HRLRT it was possible to estimate the fundamental mode to ~55 Hz (Figure 3) and achieve that goal.

Seismic data were collected along a levee located within the Rio Grande River floodplain in the San Juan Quadrangle, Texas, USA (Ivanov et al., 2017). Vertical and horizontal receivers were oriented to be sensitive to motion perpendicular to the axis of the levee (SH). Corresponding vertical and horizontal sources were used to collect in separate records each containing Rayleigh- and Love-wave energy, accordingly.

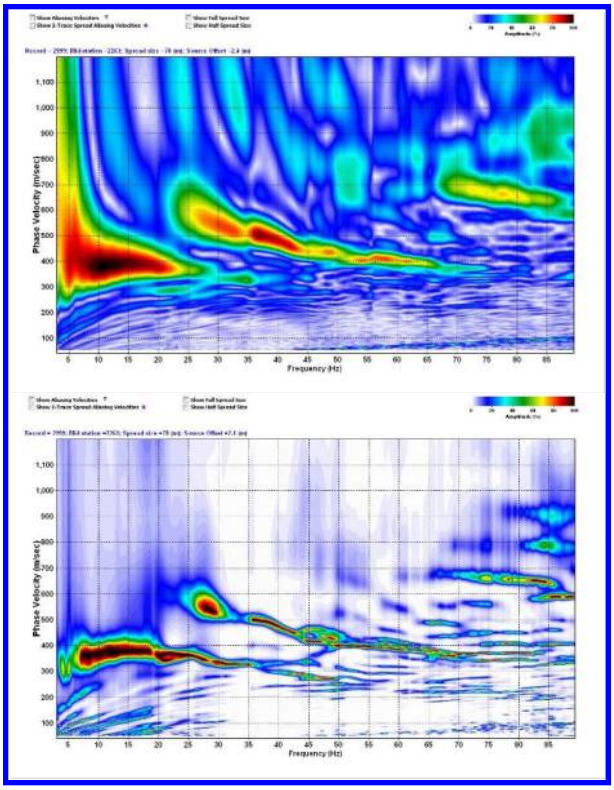

Figure 3. Rayleigh-wave dispersion-curve images of Yuma seismic data using a) the phase-shift method and b) the HRLRT.

The fundamental-mode Rayleigh-wave energy collected at the levee sites did not possess the higher frequencies necessary to sample the very shallow part of the subsurface, which included the levee core (images not shown for brevity). Love-wave analysis of some of the transverse-polarized shear-wave data using the conventional method produced encouraging dispersion trends across a frequency range from 5 Hz to over 32 Hz. However, most of the images did not contain high-frequency components of the fundamental-mode Love wave.

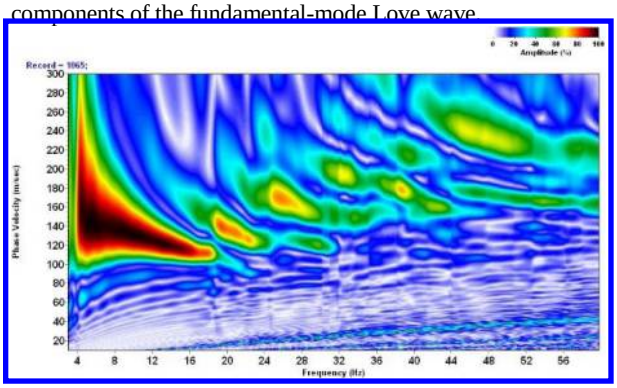

Figure 4. Love-wave dispersion curve images of record 1065 using the phase-shift method.

The HRLRT measurably extended the Love-wave fundamental-mode frequency range to > 50 Hz. Encouraged by these results, we shortened the HRLRT spread size in search of the minimal spread length for better lateral resolution, which would still remain large enough to separate the fundamental mode from the higher modes. A spread using just the first half of the optimally selected traces seemed reasonable for such a trade-off (Figure 5). HRLRT provided better opportunity for identifying higher mode. For example, it helped observe the first higher mode, not visible on the conventional image.

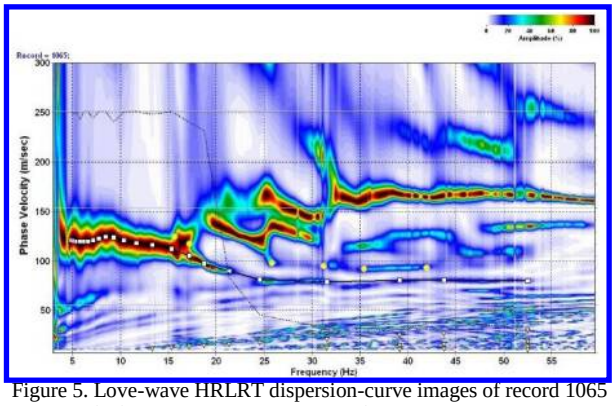

Figure 5. Love-wave HRLRT dispersion-curve images of record 1065 using half of the receivers showing the fundamental (white squares) and first higher (yellow circles) modes.

As a result, it was possible to more accurately identify higher modes. The 2D Vs image that was the product of multi-mode inversion provided greater maximum imaging depth (~10 vs 8 m) and vertical resolution (20 vs 10 layers) compared to the fundamental-mode-only 2D Vs image. (Ivanov et al., 2017). Obtaining useful dispersion-curve images with half the spread size and using twice more layers during the inversion resulted in a 2D section with four times higher resolution (i.e., two times in each direction)

Passive seismic data were collected south of the Kansas Geological Survey. Receiver station spacing was 0.61 m using 72 4.5 Hz vertical geophones. The total spread length was 43.3 m. A total of 64 records were recorded, each listening for 30 s. It was difficult to observe a noticeable dispersion-curve trend from the passive data on any of images obtained with the conventional method. That was the case even for the image that was considered the best (Figure 6a). Using HRLRT on the same record provided a noticeable fundamental-mode trend in the 20-70 Hz range (Figure 6b). To improve the signal to noise ratio we stacked the dispersion-curve images of all the records from the conventional (Figure 6c) and the HRLRT (Figure 6d) methods. It can be observed that the fundamental mode trend is hardly identifiable on the conventional image and clearly stands out on the HRLRT stack.

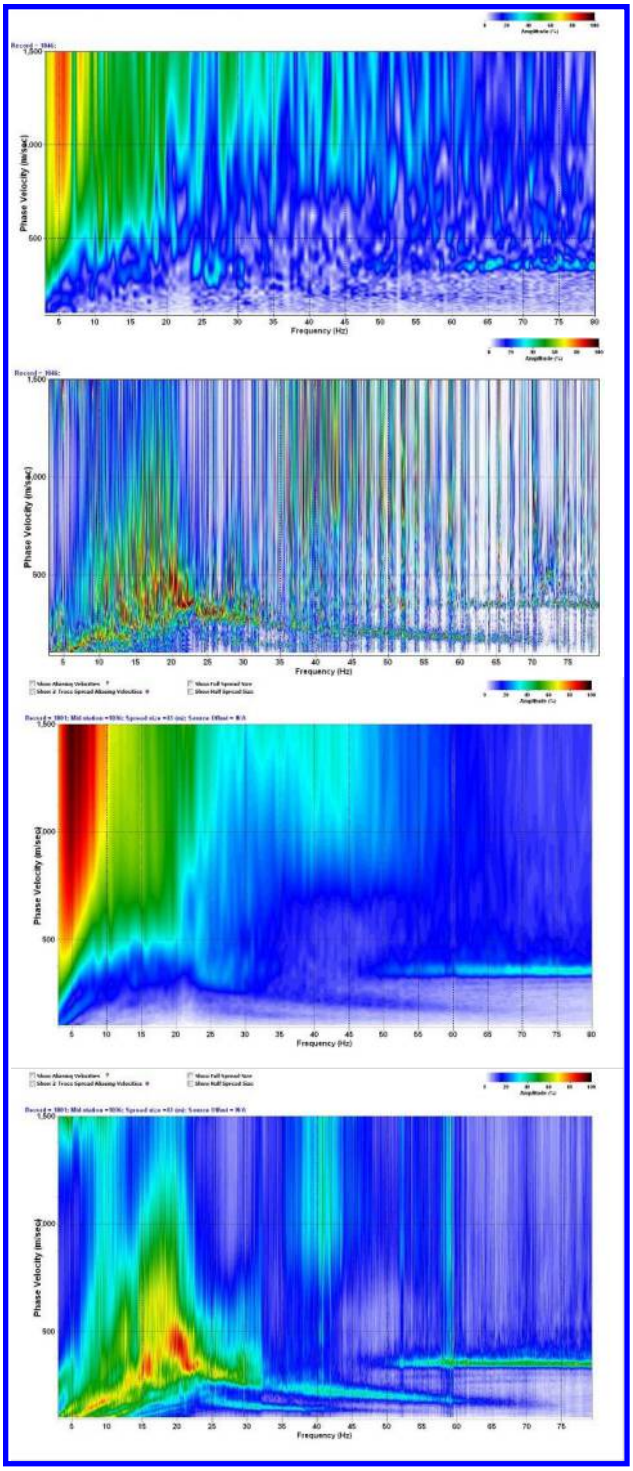

Figure 6. Passive Rayleigh-wave data dispersion-curve images of record 1046 using a) the phase-shift method and b) the HRLRT and of 68 stacked records using c) the phase-shift method and d) the HRLRT.

The ability of the HRLRT to suppress spectral leakage (Foti et al., 2015) can be shown with the 10-layer model synthetic seismic data used by (Ivanov et al., 2013). The surface wave energy trend can be identified by the red-dark red trend (Figure 7a). It can be also shown that the multiple trends in blue-light blue mimicking the main trend are related to spectral leakage. The HRLRT image is free from such noise (Figure 7b). Such noise suppression can help avoid misinterpreting residual spatial -aliasing for a real surface-wave energy trend, which can be an issue for some models.

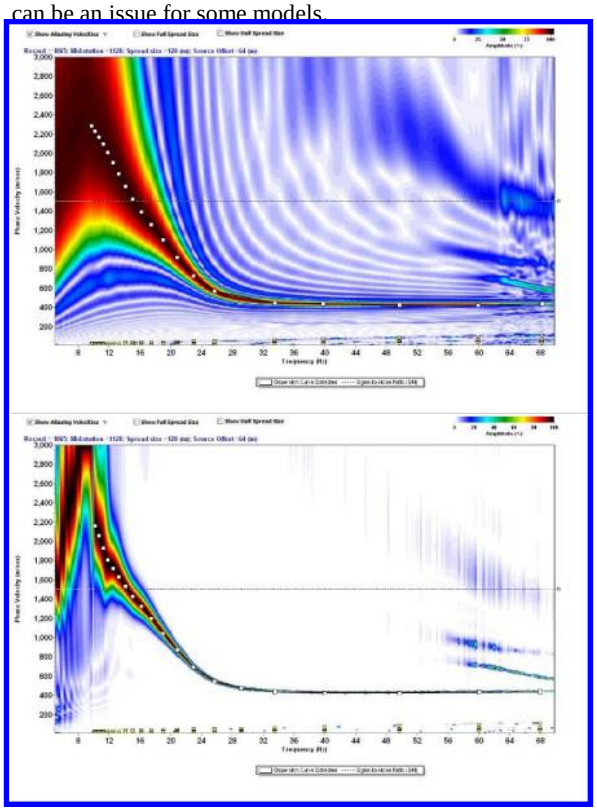

Figure 7. Rayleigh-wave dispersion-curve images of 10-layer model synthetic seismic data using a) the phase-shift method and b) the HRLRT.

Conclusions

The ability of the HRLRT to help with mode interpretation by separating surface-wave modes and reducing special aliasing noise, extending their frequency ranges, improving lateral and vertical resolution, and providing better passive data images indicates that it can be a useful tools for MASW analysis.

Acknowledgments

We also appreciate Mary Brohammer for her assistance in manuscript preparation.

EDITED REFERENCES

Note: This reference list is a copyedited version of the reference list submitted by the author. Reference lists for the 2017 SEG Technical Program Expanded Abstracts have been copyedited so that references provided with the online metadata for each paper will achieve a high degree of linking to cited sources that appear on the Web.

REFERENCES

Boaga, J., G. Cassiani, C. L. Strobbia, and G. Vignoli, 2013, Mode misidentification in Rayleigh waves: Ellipticity as a cause and a cure: Geophysics, **78**, no. 4, EN17–EN28, https://doi.org/10.1190/geo2012-0194.1.

Dal Moro, G., R. M. M. Moura, and S. S. R. Moustafa, 2015, Multi-component joint analysis of surface waves: Journal of Applied Geophysics, **119**, 128–138, https://doi.org/10.1016/j.jappgeo.2015.05.014.

Feigenbaum, D., J. Ivanov, R. Miller, S. Peterie, and S. Morton, 2016, Near-surface Qs estimations using multichannel analysis of surface waves (MASW) and the effect of nonfundamental mode energy on Q estimation: An example from Yuma proving ground, Arizona: 86th Annual International Meeting, SEG, Expanded Abstracts, 4971–4976, http://dx.doi.org/10.1190/segam2016-13873891.1.

Foti, S., G. L. Carlo, G. J. Rix, and C. Strobbia, 2015, Surface wave methods for near-surface site characterization: CRC Press.

Ikeda, T., T. Tsuji, and T. Matsuoka, 2013, Window-controlled CMP cross correlation analysis for surface waves in laterally heterogeneous media: Geophysics, **78**, no. 6, EN95–EN105, https://doi.org/10.1190/geo2013-0010.1.

Ivanov, J., C. B. Park, R. D. Miller, and J. Xia, 2000a, Mapping Poisson's ratio of unconsolidated materials from a joint analysis of surface-wave and refraction events: Symposium on the Application of Geophysics to Engineering and Environmental Problems, **13**, 11–19, https://doi.org/10.4133/1.2922727.

Ivanov, J., C. B. Park, R. D. Miller, J. Xia, J. A. Hunter, R. L. Good, and R. A. Burns, 2000b, Joint analysis of surface-wave and refraction events from river-bottom sediments: 70th Annual International Meeting, SEG, 1307–1310, http://dx.doi.org/10.1190/1.1815636.

Ivanov, J., C. B. Park, R. D. Miller, and J. H. Xia, 2005, Analyzing and filtering surface-wave energy by muting shot gathers: Journal of Environmental and Engineering Geophysics, **10**, 307–321, https://doi.org/10.2113/JEEG10.3.307.

Ivanov, J., R. D. Miller, P. Lacombe, C. D. Johnson, and J. W. Lane, 2006a, Delineating a shallow fault zone and dipping bedrock strata using multichannal analysis of surface waves with a land streamer: Geophysics, 71, A39–A42, https://doi.org/10.1190/1.2227521.

Ivanov, J., R. D. Miller, J. H. Xia, D. Steeples, and C. B. Park, 2006b, Joint analysis of refractions with surface waves: An inverse solution to the refraction-traveltime problem: Geophysics, 71, R131–R138, https://doi.org/10.1190/1.2360226.

Ivanov, J., T. J. Schwenk, R. D. Miller, and S. Peterie, 2013, Dispersion-curve imaging nonuniqueness studies from multi-channel analysis of surface waves (MASW) using synthetic seismic data: 83rd Annual International Meeting, SEG, Expanded Abstracts, 1794–1800, http://dx.doi.org/10.1190/segam2013-0425.1.

Ivanov, J., G. Tsoflias, R. D. Miller, S. Peterie, S. Morton, and J. Xia 2016, Impact of density information on Rayleigh surface wave inversion results: Journal of Applied Geophysics, 135, 43–54, https://doi.org/10.1016/j.jappgeo.2016.09.011.

Ivanov, J., R. D. Miller, D. Feigenbaum, S. L. C. Morton, S. Peterie, and J. B. Dunbar, 2017, Revisiting levees in southern Texas using Love-wave multichannel analysis of surface waves with the high-

resolution linear Radon transform: Interpretation, 5, T287–T298, https://doi.org/10.1190/INT-2016-0044.1.
Kaufmann, R. D., J. H. Xia, R. C. Benson, L. B. Yuhr, D. W. Casto, and C. B. Park, 2005, Evaluation of MASW data acquired with a hydrophone streamer in a shallow marine environment: Journal of Environmental and Engineering Geophysics, 10, 87–98, https://doi.org/10.2113/JEEG10.2.87.
Luo, Y. H., J. H. Xia, R. D. Miller, Y. X. Xu, J. P. Liu, and Q. S. Liu, 2008, Rayleigh-wave dispersive energy imaging using a high-resolution linear Radon transform: Pure and Applied Geophysics, 165, 903–922, https://doi.org/10.1007/s00024-008-0338-4.
Miller, R. D., J. Xia, C. B. Park, J. C. Davis, W. T. Shefchik, and L. Moore, 1999a, Seismic techniques to delineate dissolution features in the upper 1000 ft at a power plant site: 69th Annual International Meeting, SEG, Expanded Abstracts, 492–495, http://dx.doi.org/10.1190/1.1821061.
Miller, R. D., J. Xia, C. B. Park, and J. M. Ivanov, 1999b, Multichannel analysis of surface waves to map bedrock: The Leading Edge, 18, 1392–1396, https://doi.org/10.1190/1.1438226.
Miller, R. D., T. S. Anderson, J. Ivanov, J. C. Davis, R. Olea, C. Park, D. W. Steeples, M. L. Moran, and J. Xia, 2003, 3-D characterization of seismic properties at the smart weapons test range, YPG: 73rd Annual International Meeting, SEG, Expanded Abstracts, 22, 1195–1198, http://dx.doi.org/10.1190/1.1817493.
Pan, Y. D., J. H. Xia, and C. Zeng, 2013, Verification of correctness of using real part of complex root as Rayleigh-wave phase velocity with synthetic data: Journal of Applied Geophysics, 88, 94–100, https://doi.org/10.1016/j.jappgeo.2012.09.012.
Park, C. B., R. D. Miller, and J. Xia, 1998, Imaging dispersion curves of surface waves on multi-channel record: 68th Annual International Meeting, SEG, Expanded Abstracts, 1377–1380, http://dx.doi.org/10.1190/1.1820161.
Park, C. B., R. D. Miller, J. Xia, J. Ivanov, G. V. Sonnichsen, J. A. Hunter, R. L. Good, R. A. Burns, and H. Christian, 2005, Underwater MASW to evaluate stiffness of water-bottom sediments: The Leading Edge, 24, 724–728, https://doi.org/10.1190/1.1993267.
Piatti, C., L. V. Socco, D. Boiero, and S. Foti, 2013, Constrained 1D joint inversion of seismic surface waves and P-refraction traveltimes: Geophysical Prospecting, 61, 77–93, https://doi.org/10.1111/j.1365-2478.2012.01071.x.
Ryden, N., C. B. Park, P. Ulriksen, and R. D. Miller, 2004, Multimodal approach to seismic pavement testing: Journal of Geotechnical and Geoenvironmental Engineering, 130, 636–645, https://doi.org/10.1061/(ASCE)1090-0241(2004)130:6(636).
Socco, L. V., S. Foti, and D. Boiero, 2010, Surface-wave analysis for building near-surface velocity models — Established approaches and new perspectives, 75, 75A83–75A102, https://doi.org/10.1190/1.3479491.
Song, Y. Y., J. P. Castagna, R. A. Black, and R. W. Knapp, 1989, Sensitivity of near-surface shear-wave velocity determination from rayleigh and love waves: 59th Annual International Meeting, SEG, Expanded Abstracts, 8, 509–512, http://dx.doi.org/10.1190/1.1889669.
Suto, K., 2013, MASW surveys in landfill sites in Australia: The Leading Edge, 32, 674–678, https://doi.org/10.1190/tle32060674.1.
Tsoflias, G. P., J. Ivanov, S. Anandakrishnan, and R. D. Miller, 2008, Use of active source seismic surface waves in glaciology: Symposium on the Application of Geophysics to Engineering and Environmental Problems, 21, 1240–1243, https://doi.org/10.4133/1.2963234.
Tsuji, T., T. A. Johansen, B. O. Ruud, T. Ikeda, and T. Matsuoka, 2012, Surface-wave analysis for identifying unfrozen zones in subglacial sediments: Geophysics, 77, En17–En27, https://doi.org/10.1190/geo2011-0222.1.

Xia, J., R. D. Miller, C. B. Park, J. A. Hunter, and J. B. Harris, 2000, Comparing shear-wave velocity profiles from MASW with borehole measurements in unconsolidated sediments, Fraser River Delta, B.C., Canada: Journal of Environmental and Engineering Geophysics, 5, 1–13, https://doi.org/10.4133/JEEG5.3.1.

Xia, J., C. Shen, and Y. Xu, 2013, Near-surface shear-wave velocities and quality factors derived from high-frequency surface waves: The Leading Edge, 32, 612–618, https://doi.org/10.1190/tle32060612.1.

Xia, J. H., R. D. Miller, and C. B. Park, 1999, Estimation of near-surface shear-wave velocity by inversion of Rayleigh waves: Geophysics, 64, 691–700, https://doi.org/10.1190/1.1444578.

Xu, Y. X., J. H. Xia, and R. D. Miller, 2007, Numerical investigation of implementation of air-earth boundary by acoustic-elastic boundary approach: Geophysics, 72, Sm147–Sm153, https://doi.org/10.1190/1.2753831.

Zeng, C., J. H. Xia, R. D. Miller, G. P. Tsoflias, and Z. J. Wang, 2012, Numerical investigation of MASW applications in presence of surface topography: Journal of Applied Geophysics, 84, 52–60. https://doi.org/10.1016/j.jappgeo.2012.06.004.